

W  
N90-12477

213-92

243228

150

# FLARE MODEL SENSITIVITY

# OF THE BALMER SPECTRUM

A. Falchi<sup>1</sup>, R. Falciani<sup>2</sup>, L.A. Smaldone<sup>3</sup> and G.P. Tozzi<sup>1</sup>

<sup>1</sup> Osservatorio Astrofisico di Arcetri  
Largo E. Fermi 5 - 50125 Firenze (Italy)

<sup>2</sup> Dipartimento di Astronomia  
Largo E. Fermi 5 - 50125 Firenze (Italy)

<sup>3</sup> Dipartimento di Scienze Fisiche  
Pad. 19-20 Mostra d'Oltremare - 80125 Napoli (Italy)

## Introduction.

Careful studies of various chromospheric spectral signatures are very important in order to explore their possible "sensitivity" to the modifications of the thermodynamic quantities produced by the flare occurrence.

Pioneer work of Canfield and co-workers (Canfield et al., 1984) have shown how the  $H_\alpha$  behaviour is able to indicate different changes in the atmospheric parameters structure associated to the flare event.

We decided to study the behaviour of the highest Balmer lines and of the Balmer continuum in different solar flare model atmospheres. These spectral features, originating in the deep photosphere in a quiet area, may have a sensitivity different from  $H_\alpha$  to the modification of a flare atmosphere.

The details of the method used to compute the Stark profile of the higher Balmer lines ( $n \geq 6$ ) and their merging have been extensively given elsewhere (Donati-Falchi et al., 1985; Falchi et al., 1989).

We used the models developed by Ricchiazzi in his thesis (1982) who evaluated the chromospheric response to both the non-thermal electron flux, for energy  $> 20\text{KeV}$ , ( $F_{20}$ ) and to the thermal conduction ( $F_c$ ). The effect of the coronal pressure values ( $P_0$ ) at the apex of the flare loop is also included.

## Results

In order to compare our results to those obtained by Canfield et al. (1984) for the  $H_\alpha$  profiles, we will separately explore the effects produced on the considered spectral features by the changes of the three input parameters of the considered flare atmospheres. The various models will be hereafter referred to as M:A:B:C in which  $F_{20} = 10^A \text{erg cm}^{-2} \text{sec}^{-1}$ ,  $F_c = 10^B \text{erg cm}^{-2} \text{sec}^{-1}$ , and  $P_0 = 10^C \text{dyne cm}^{-2}$ .

### *Effects of non-thermal electron flux $F_{20}$*

We considered two regimes of  $P_0$ :

$P_0 = 1 \text{dyne cm}^{-2}$  (low coronal pressure) and

$P_0 = 10^2 \text{dyne cm}^{-2}$  (nominal coronal pressure) in order to better understand the influences due to the  $F_{20}$  variations. The nominal value for  $F_c$  is assumed to be  $10^7 \text{erg cm}^{-2} \text{sec}^{-1}$ . The dependence on  $F_{20}$  of our spectral signatures is roughly the same for the two  $P_0$  regimes: the Balmer continuum increases with  $F_{20}$  enhancements while the Balmer lines intensity seems to be rather insensitive. With the highest  $F_{20}$  values we only notice broader line profiles. The results obtained with the models M:9:7:2 and M:10:7:2 and M:11:7:2 are illustrated in Figures 1 and 2.

### *Effects of coronal pressure $P_0$*

We considered three different values of  $P_0$ :

$$P_0 = 1, 10^2, 10^3 \text{ dyne cm}^{-2}$$

$$\text{with } F_{20} = 10^{10} \text{ erg cm}^{-2} \text{ sec}^{-1},$$

$$\text{and } F_c = 10^7 \text{ erg cm}^{-2} \text{ sec}^{-1}.$$

The Balmer continuum is quite sensitive ( $\Delta I \simeq 2.$ ) to the value of the coronal pressure when  $P_0$  is ranging from 1 to  $10^2$ , while, in the interval  $10^2 - 10^3$ , the intensity remains practically the same but the slope. In fact all the highest Balmer lines are in absorption for  $P_0 \leq 10^2$  and become in emission with very broad wings for  $P_0 = 10^3$  and in this case the merging of the highest Balmer lines changes the slope of the continuum. These results are shown in Figures 3 and 4.

### *Effects of thermal conductive flux $F_c$*

We considered 2 different regimes of  $P_0$ :

$$P_0 = 1 \text{ dyne cm}^{-2} \text{ with } F_c = 10^6, 10^7, 10^8 \text{ erg cm}^{-2} \text{ sec}^{-1}$$

$$P_0 = 10^2 \text{ dyne cm}^{-2} \text{ with } F_c = 10^7, 10^8 \text{ erg cm}^{-2} \text{ sec}^{-1}$$

For all these models a value of  $F_{20} = 10^{10} \text{ erg cm}^{-2} \text{ sec}^{-1}$  is assumed. For  $P_0$  ranging from 1 to  $10^2$  the Balmer continuum decreases as  $F_c$  increases. The highest Balmer lines are in absorption with broad wings and a central narrow emission core. The Balmer line intensities seem to be quite insensitive to the  $F_c$  values increase. The results for models M:10:7:2 and M:10:8:2 are shown in Figures 5 and 6.

The  $T_e(h)$  and  $N_e(h)$  distributions for all the considered models are shown in Figures 7, 8 and 9.

## CONCLUSIONS

### Balmer Continuum

- its strong increase in intensity unambiguously reflects high values of  $F_{20}$ . This signature is equivalent to the  $H_\alpha$  wings sensitivity found by Canfield et al. (1984);
- it decreases when  $F_c$  increases;

### Balmer Lines

- broad and relevant wings in Balmer lines indicate a high  $F_{20}$  value as already found for  $H_\alpha$ ;
- strong variations in intensity can be due to a  $P_0$  increase ( $> 10^2$ );
- they seem to be quite insensitive to  $F_c$  variations.

Calculations of the Na-D lines profiles are in progress. These spectral features may be used to disentangle the remaining ambiguities still present in  $H_\alpha$  and Balmer continuum.

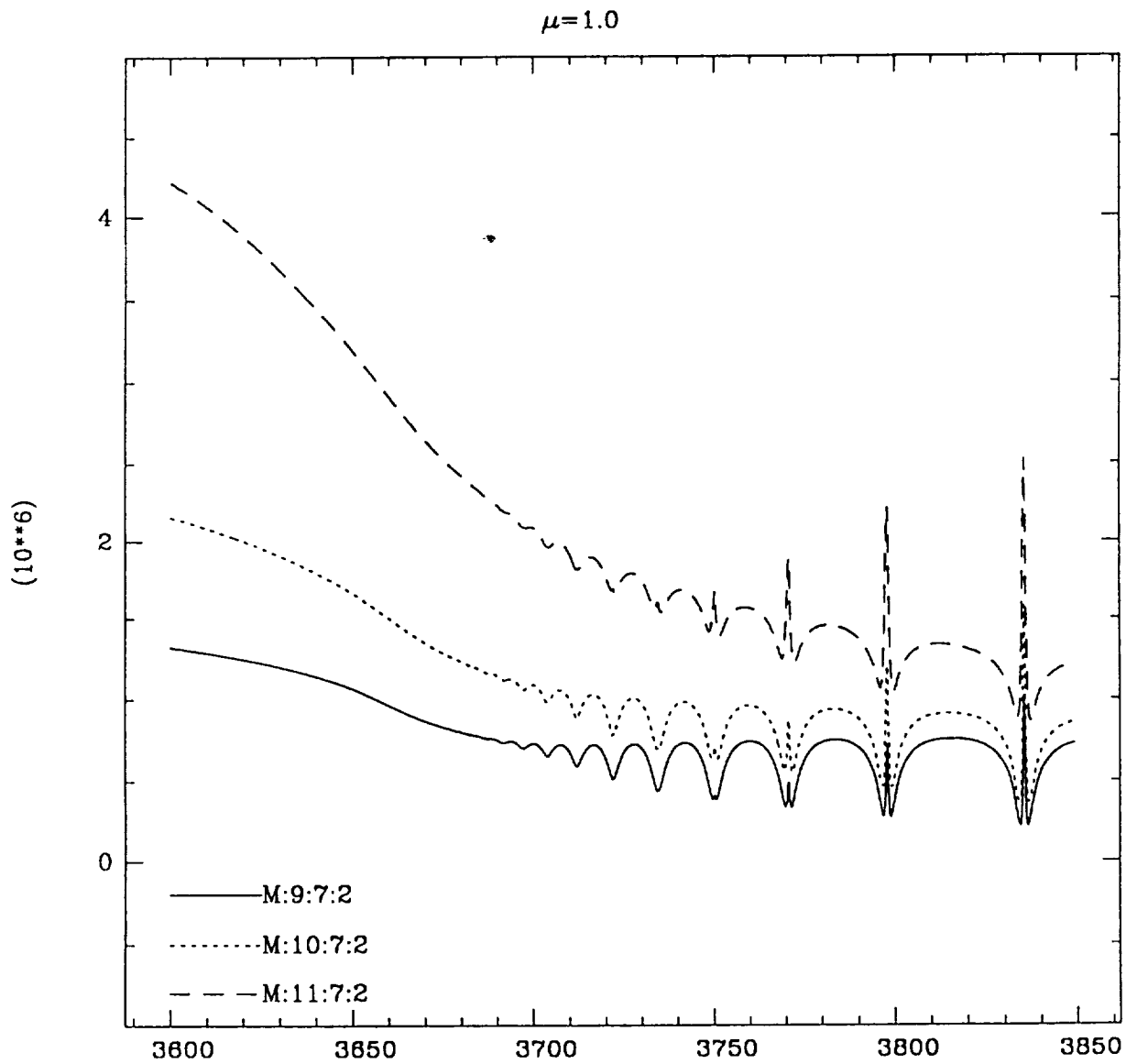


Fig. 1 - Flare net emission in the spectral range 3600 - 3850 Å computed for the labelled flare models (see the text for their meaning).

Units are  $10^6 \text{ erg sec}^{-1} \text{ cm}^{-2} \text{ ster}^{-1}$ .

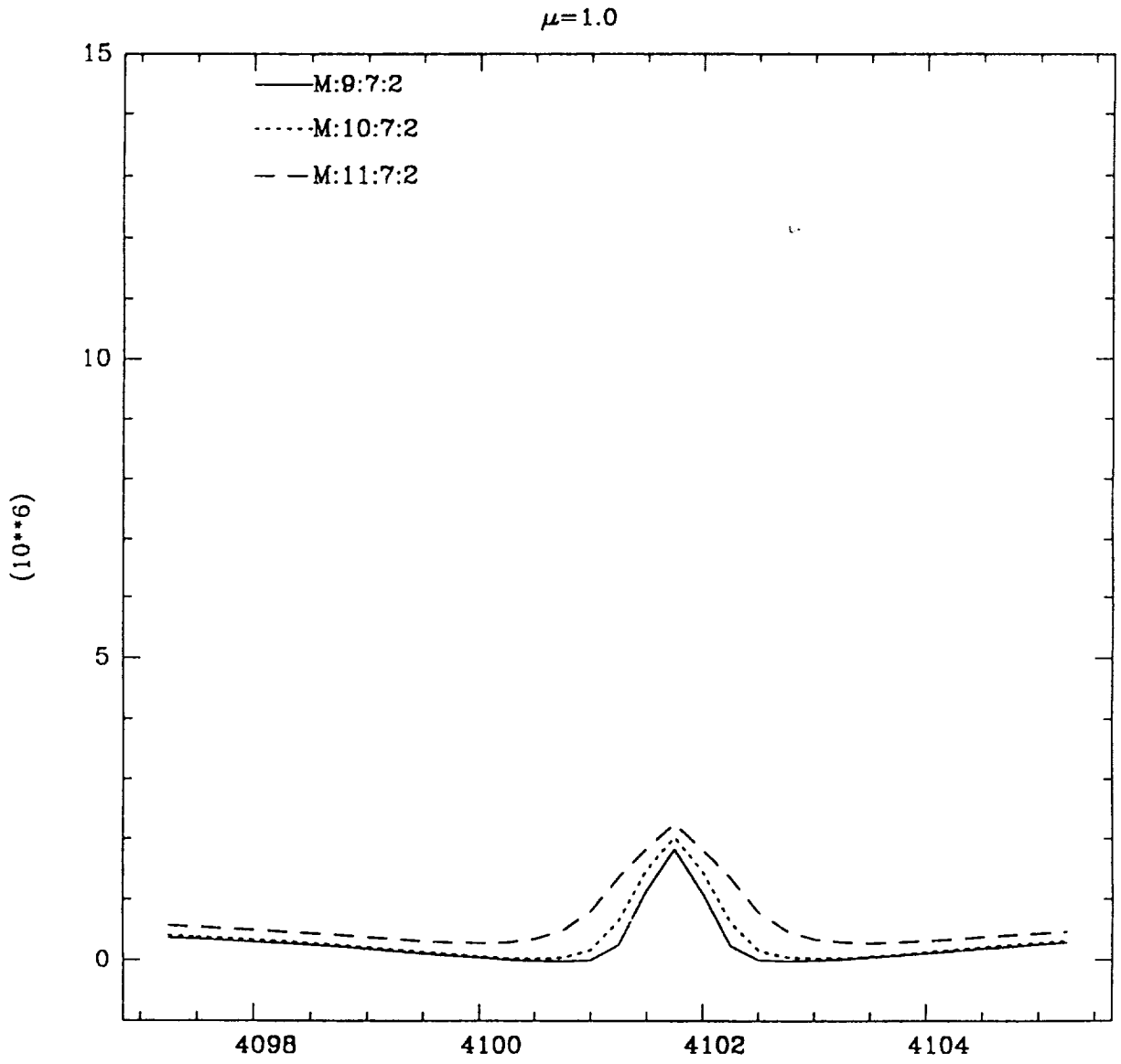


Fig. 2 - Flare net emission in  $H_{\delta}$  line computed for the labelled flare models.

Units are  $10^6 \text{ erg sec}^{-1} \text{ cm}^{-2} \text{ ster}^{-1}$ .



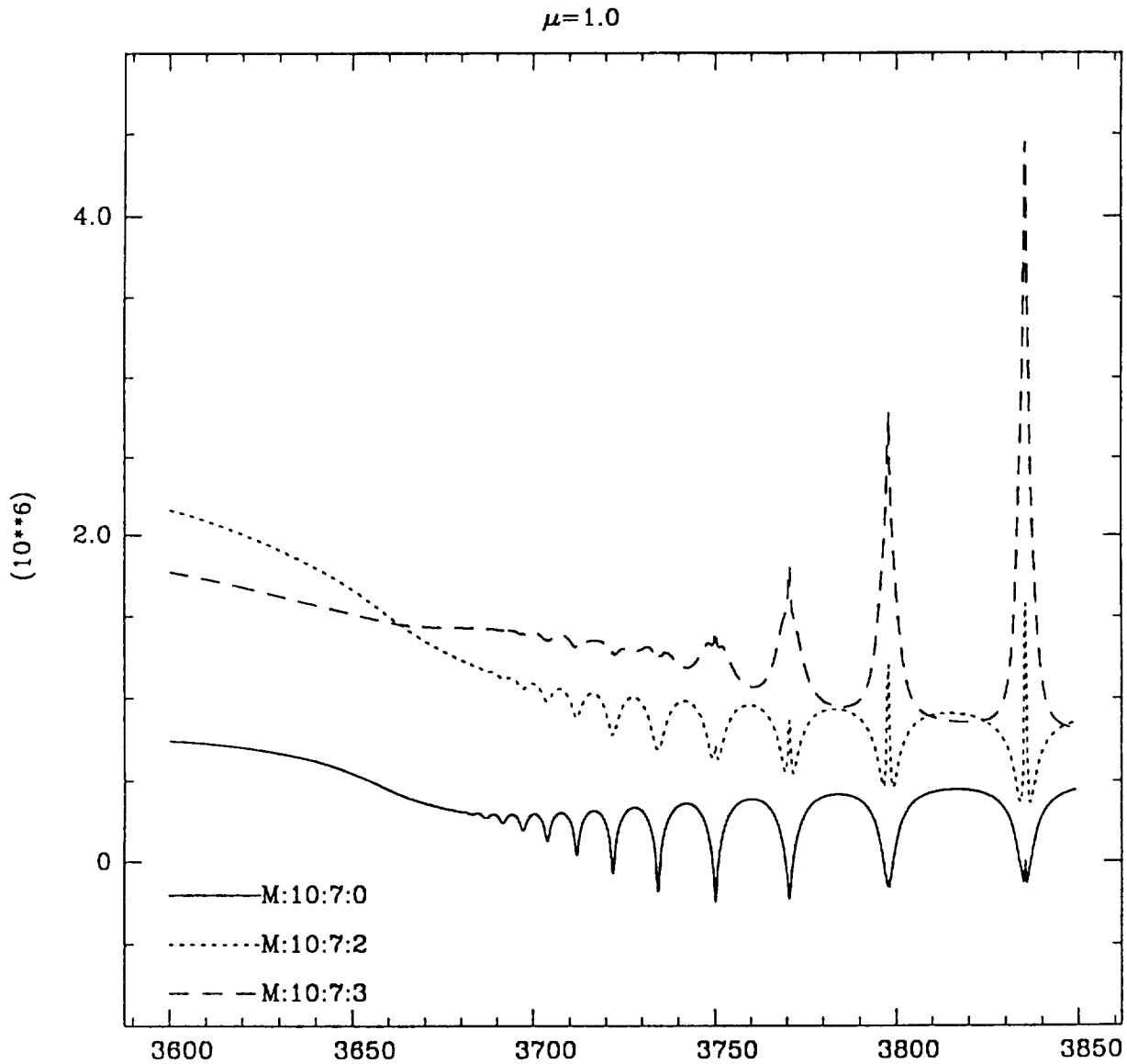


Fig. 3 - Flare net emission in the spectral range 3600 - 3850 Å computed for the labelled flare models (see the text for their meaning).

Units are  $10^6 \text{ erg sec}^{-1} \text{ cm}^{-2} \text{ ster}^{-1}$ .

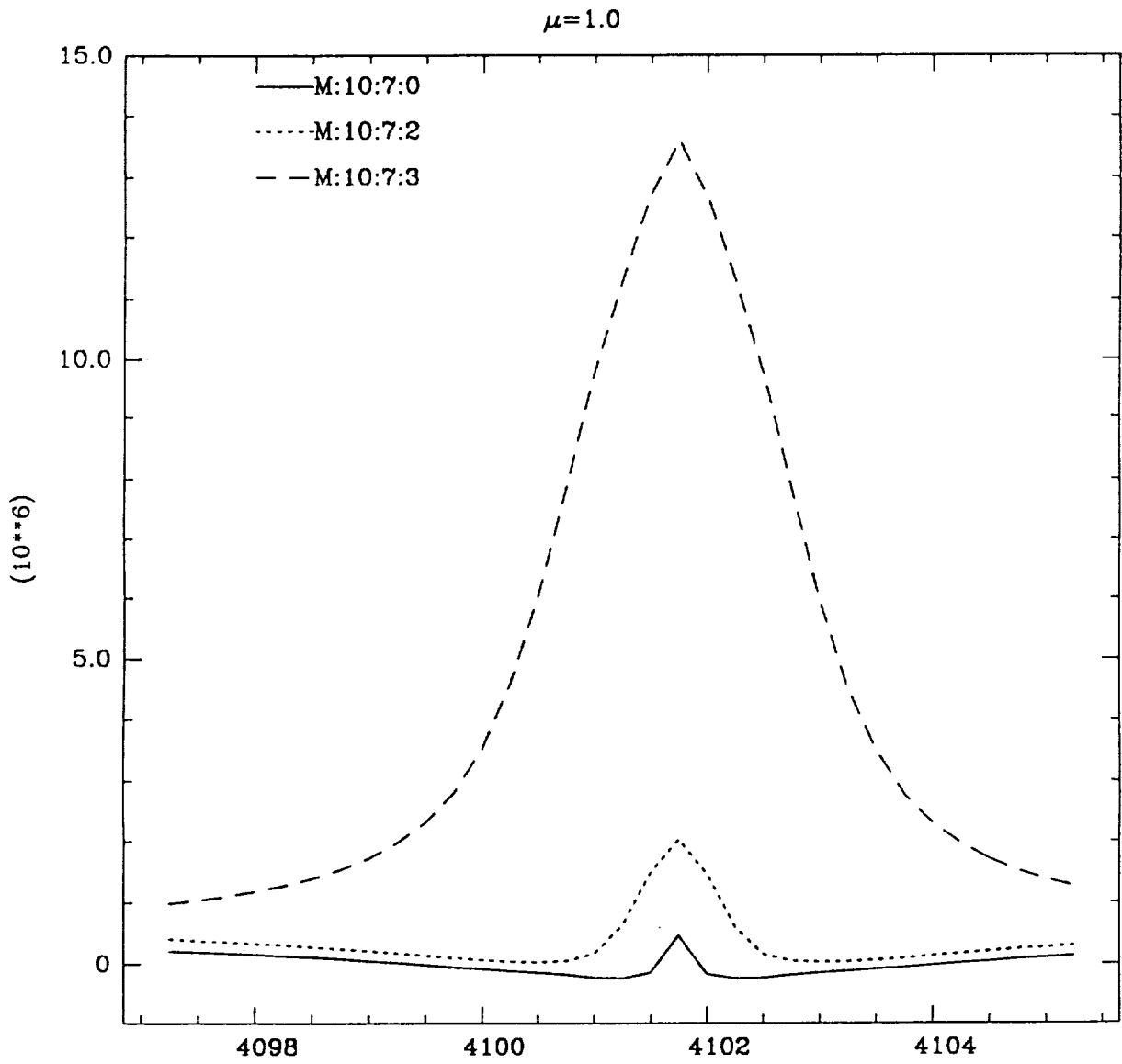


Fig. 4 - Flare net emission in  $H_{\delta}$  line computed for the labelled flare models.

Units are  $10^6 \text{ erg sec}^{-1} \text{ cm}^{-2} \text{ ster}^{-1}$

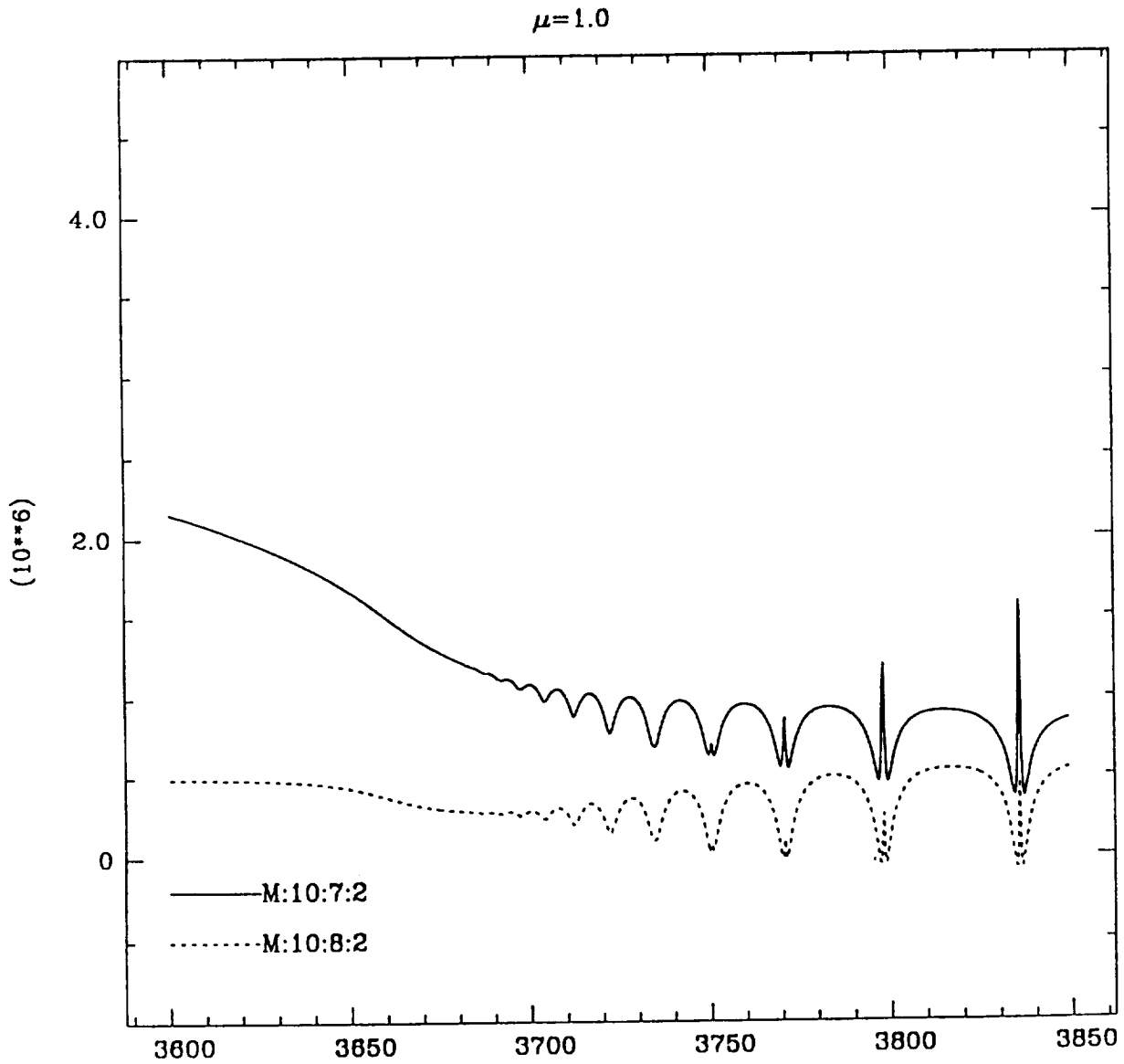


Fig. 5 - Flare net emission in the spectral range 3600 - 3850 Å computed for the labelled flare models (see the text for their meaning).

Units are  $10^6 \text{ erg sec}^{-1} \text{ cm}^{-2} \text{ ster}^{-1}$ .

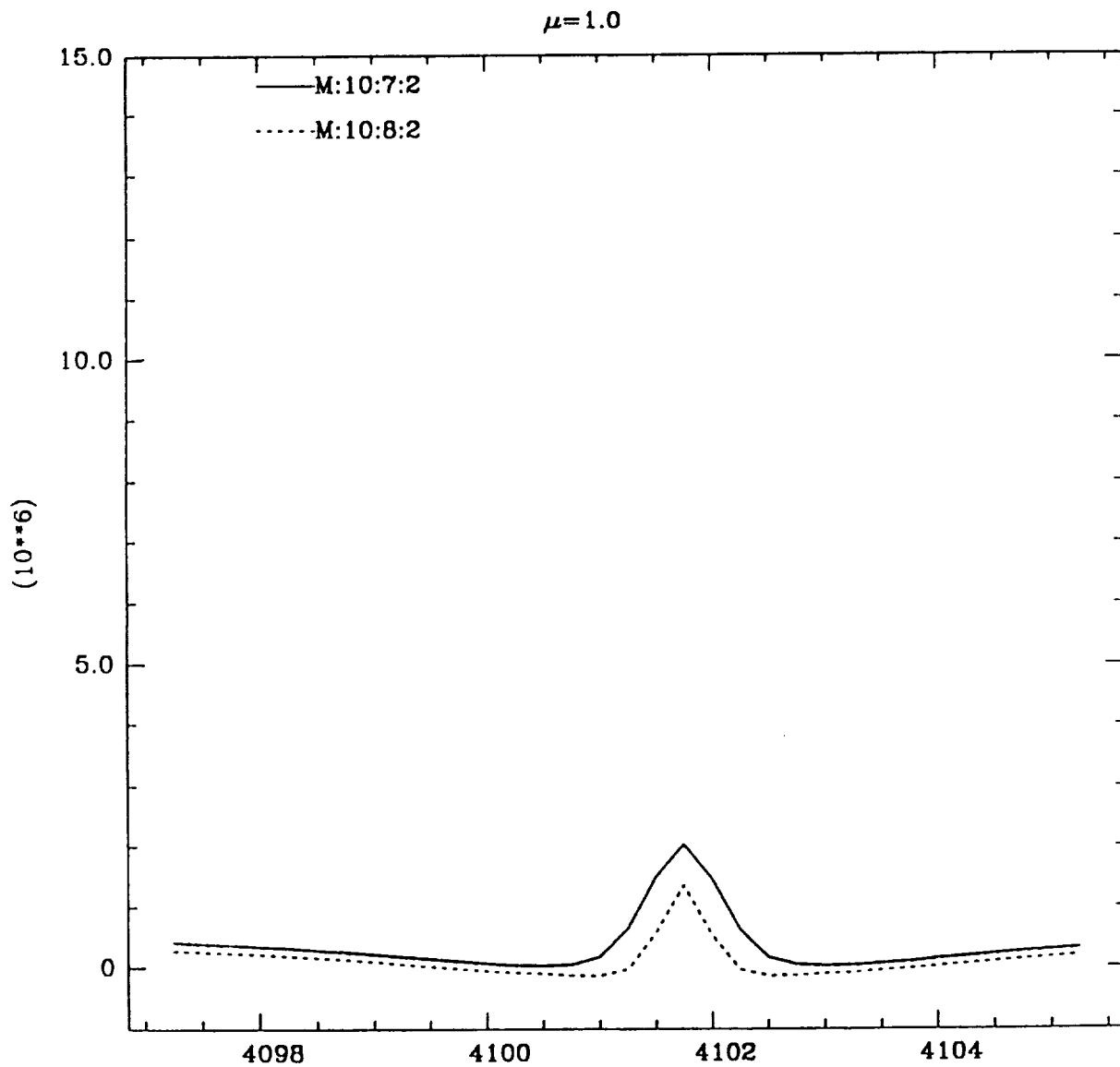


Fig. 6 - Flare net emission in  $H_{\delta}$  line computed for the labelled flare models.

Units are  $10^6 \text{ erg sec}^{-1} \text{ cm}^{-2} \text{ ster}^{-1}$

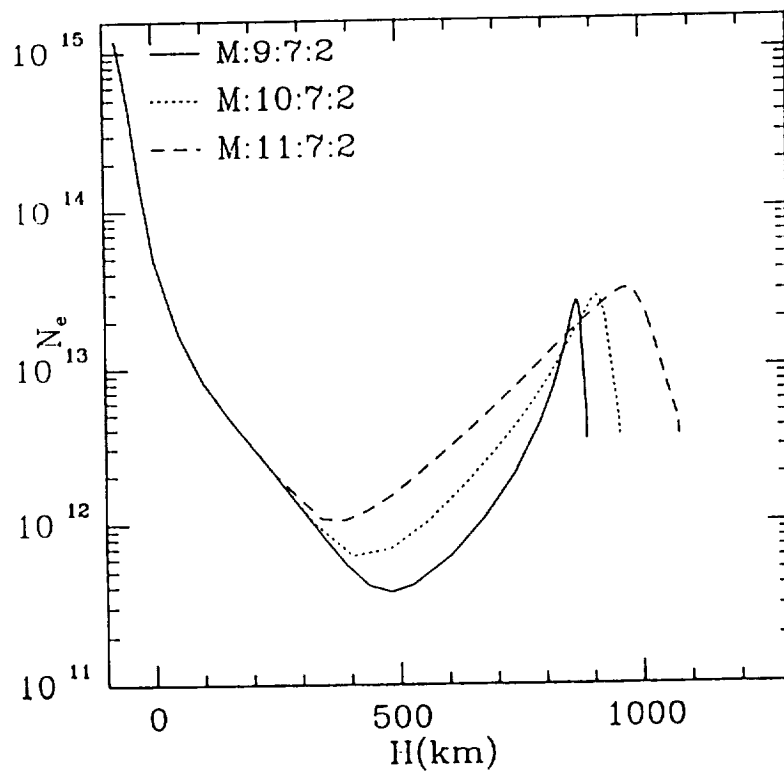
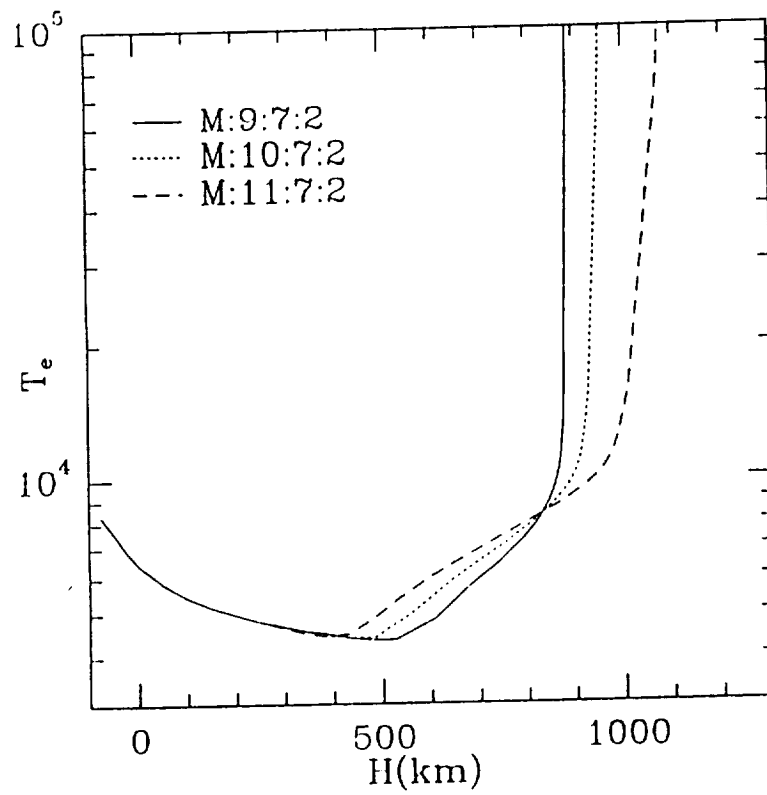


Fig. 7 - Log  $T_e$  and Log  $N_e$  distributions vs geometrical height.

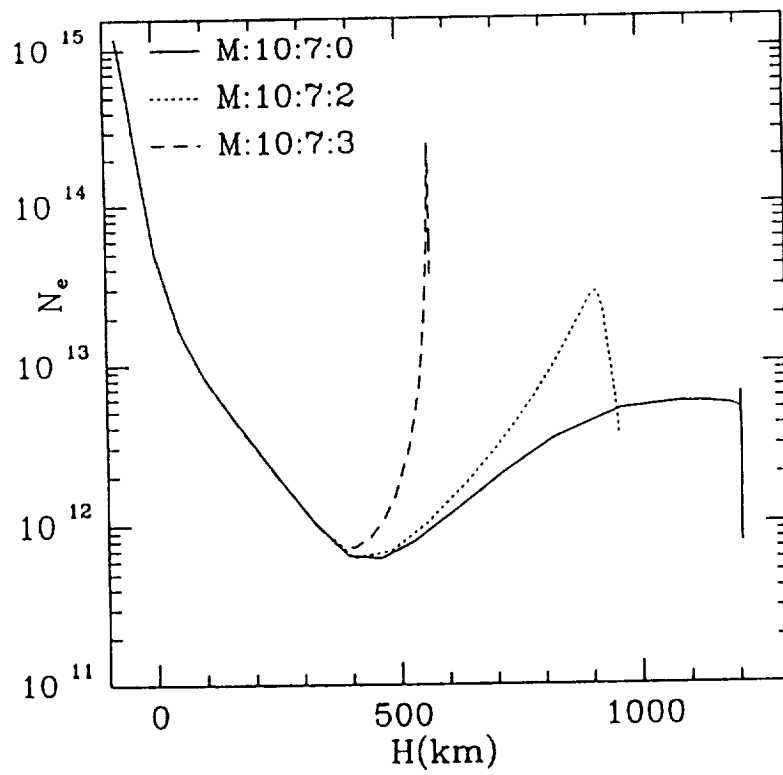
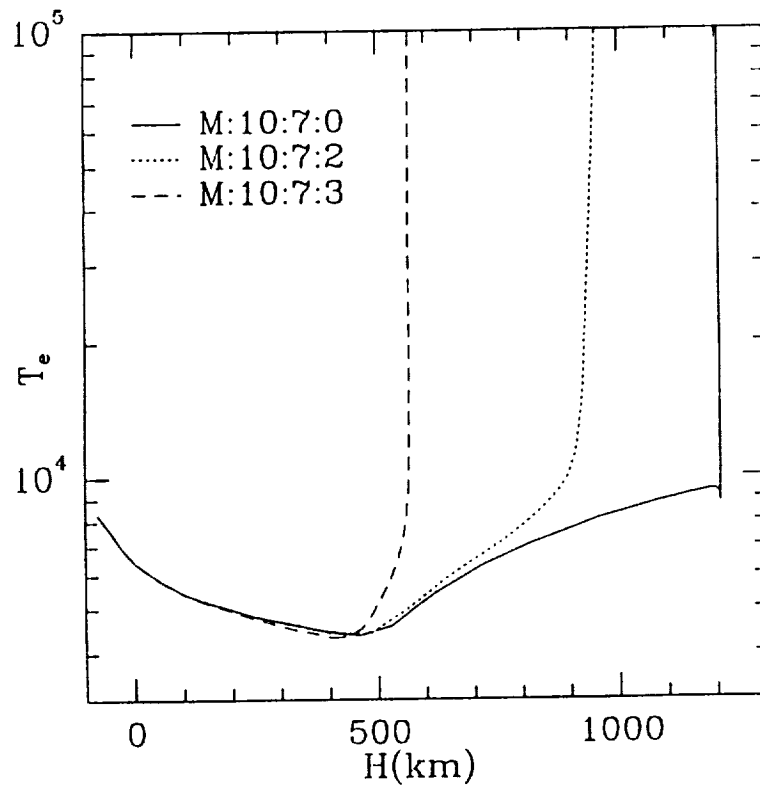


Fig. 8 - Log  $T_e$  and Log  $N_e$  distributions vs geometrical height.

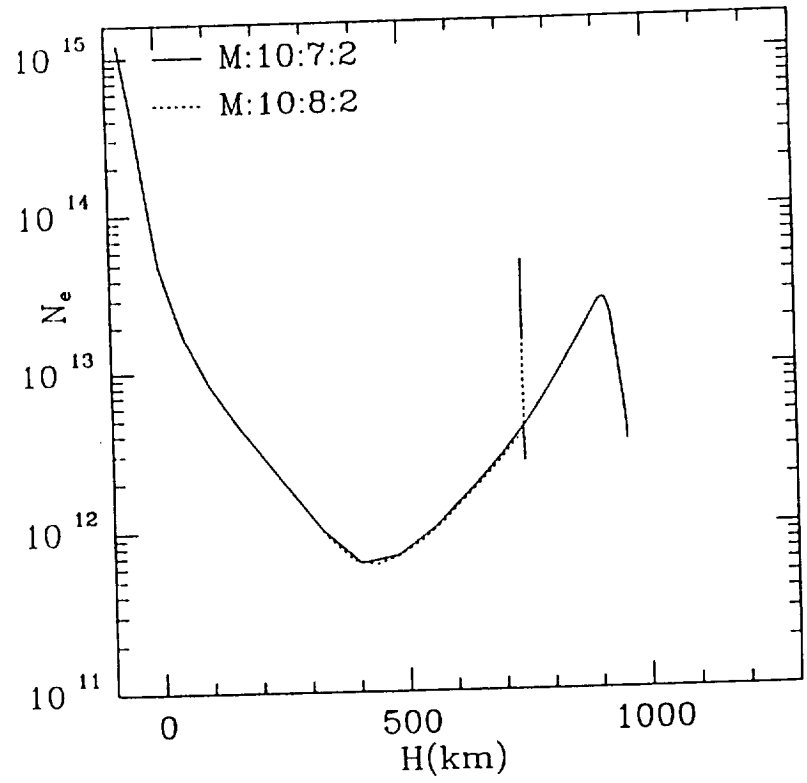
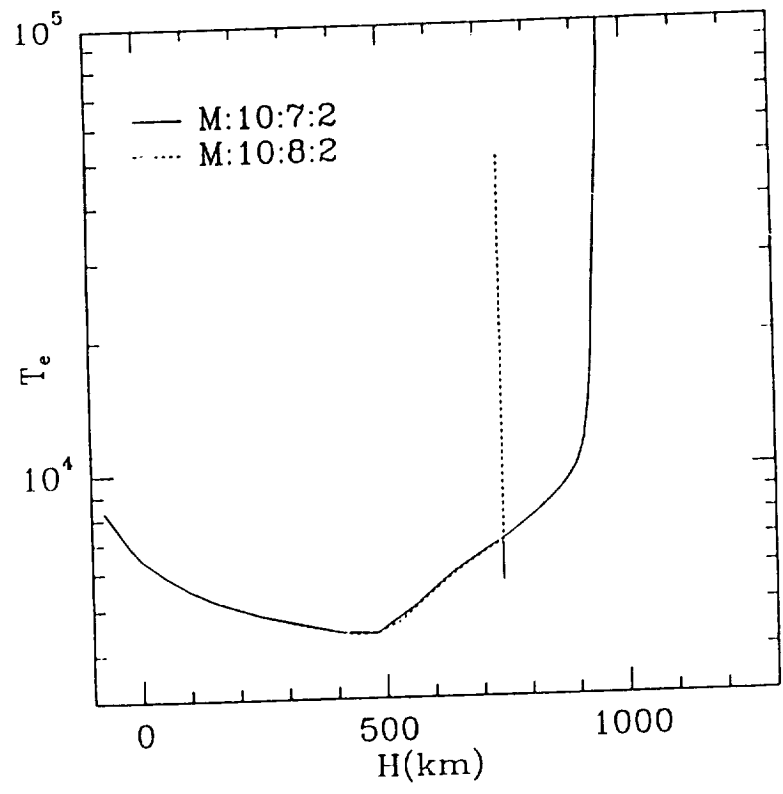


Fig. 9 - Log  $T_e$  and Log  $N_e$  distributions vs geometrical height.